p53 isoforms regulate aging- and tumor-associated replicative senescence in T lymphocytes

Abdul M. Mondal,[1] Izumi Horikawa,[1] Sharon R. Pine,[1,2] Kaori Fujita,[1] Katherine M. Morgan,[2] Elsa Vera,[3] Sharlyn J. Mazur,[4] Ettore Appella,[4] Borivoj Vojtesek,[5] Maria A. Blasco,[3] David P. Lane,[6] and Curtis C. Harris[1]

[1]Laboratory of Human Carcinogenesis, Center for Cancer Research, National Cancer Institute, NIH, Bethesda, Maryland, USA. [2]Department of Medicine, UMDNJ/Robert Wood Johnson Medical School, The Cancer Institute of New Jersey, New Brunswick, New Jersey, USA. [3]Telomeres and Telomerase Group/Molecular Oncology Programme, Centro Nacional de Investigaciones Oncológicas, C/Melchor Fernández Almagro, Madrid, Spain. [4]Laboratory of Cell Biology, Center for Cancer Research, National Cancer Institute, NIH, Bethesda, Maryland, USA. [5]Regional Centre for Applied Molecular Oncology, Masaryk Memorial Cancer Institute, Brno, Czech Republic. [6]Institute of Molecular and Cell Biology, Agency for Science, Technology and Research (A*STAR), Singapore.

Cellular senescence contributes to aging and decline in tissue function. p53 isoform switching regulates replicative senescence in cultured fibroblasts and is associated with tumor progression. Here, we found that the endogenous p53 isoforms Δ133p53 and p53β are physiological regulators of proliferation and senescence in human T lymphocytes in vivo. Peripheral blood $CD8^+$ T lymphocytes collected from healthy donors displayed an age-dependent accumulation of senescent cells ($CD28^-CD57^+$) with decreased Δ133p53 and increased p53β expression. Human lung tumor-associated $CD8^+$ T lymphocytes also harbored senescent cells. Cultured $CD8^+$ blood T lymphocytes underwent replicative senescence that was associated with loss of CD28 and Δ133p53 protein. In poorly proliferative, Δ133p53-low $CD8^+CD28^-$ cells, reconstituted expression of either Δ133p53 or CD28 upregulated endogenous expression of each other, which restored cell proliferation, extended replicative lifespan and rescued senescence phenotypes. Conversely, Δ133p53 knockdown or p53β overexpression in $CD8^+CD28^+$ cells inhibited cell proliferation and induced senescence. This study establishes a role for Δ133p53 and p53β in regulation of cellular proliferation and senescence in vivo. Furthermore, Δ133p53-induced restoration of cellular replicative potential may lead to a new therapeutic paradigm for treating immunosenescence disorders, including those associated with aging, cancer, autoimmune diseases, and HIV infection.

Introduction

Cellular senescence is sustained cell proliferation arrest induced either by telomere attrition (replicative senescence; refs. 1, 2) or by cellular stresses such as oncogene activation (stress-induced premature senescence; ref. 3). Senescent cells accumulate in vivo during aging and are assumed to contribute actively to aging phenotypes (4–6). For example, cellular senescence of normal tissue stem cells results in impaired tissue regeneration and homeostasis (7). In addition, secreted factors from senescent cells, such as proinflammatory cytokines, can cause adverse effects on surrounding nonsenescent cells (so-called *senescence-associated secretory phenotypes* [SASPs]; refs. 6, 8, 9). Recently, immune-mediated clearance of senescent cells in vivo has been shown to be a critical mechanism that limits development of cancer and other disorders (10, 11), providing further evidence for the active role of in vivo senescent cells in aging-associated pathologies. These findings suggest that senescent cells themselves and their associated phenotypes can be therapeutic targets in various human diseases (6).

The p53 signaling network plays a critical role in the induction of cellular senescence (12). The human *TP53* gene encodes, in addition to full-length p53 protein (p53FL), at least 13 natural isoforms due to alternative splicing and usage of alternative promoters (13). Among them are p53β, a C-terminally truncated isoform that cooperates with p53FL, and Δ133p53, an N-terminally truncated isoform that inhibits p53FL in a dominant-negative manner (14). In normal human fibroblasts cultured in vitro, p53β accelerates and Δ133p53 represses replicative senescence (15), consistent with their modes of functional interaction with p53FL. Premalignant colon adenomas with pathologically induced senescent cells in vivo also showed a specific profile of p53 isoform expression (i.e., elevated levels of p53β and reduced levels of Δ133p53), the loss of which was associated with malignant progression to colon carcinomas (15). We recently discovered that SRSF3, a member of a highly conserved family of splicing factors, regulates the generation of p53β during replicative senescence (16). It is of great interest to investigate whether these p53 isoforms function as regulators of physiological cellular senescence in vivo and whether they can be a therapeutic target for functional restoration of senescent or near-senescent cells.

The difficulty in isolating or genetically manipulating senescent cells in human solid tissues has hampered better understanding of in vivo roles of senescent cells and development of cell-based methods to reverse physiological and pathological aging phenotypes in humans. $CD8^+$ T lymphocytes, which can be easily isolated and analyzed ex vivo via flow cytometry or other antibody-based methods and can be genetically modified in vitro (17), provide a useful cell model to study cellular senescence in vivo. Circulating $CD8^+$ T lymphocytes in blood are at various differentiation states, from

Authorship note: Abdul M. Mondal and Izumi Horikawa contributed equally to this work.

Conflict of interest: The authors have declared that no conflict of interest exists.

Citation for this article: *J Clin Invest.* 2013;123(12):5247–5257. doi:10.1172/JCI70355.

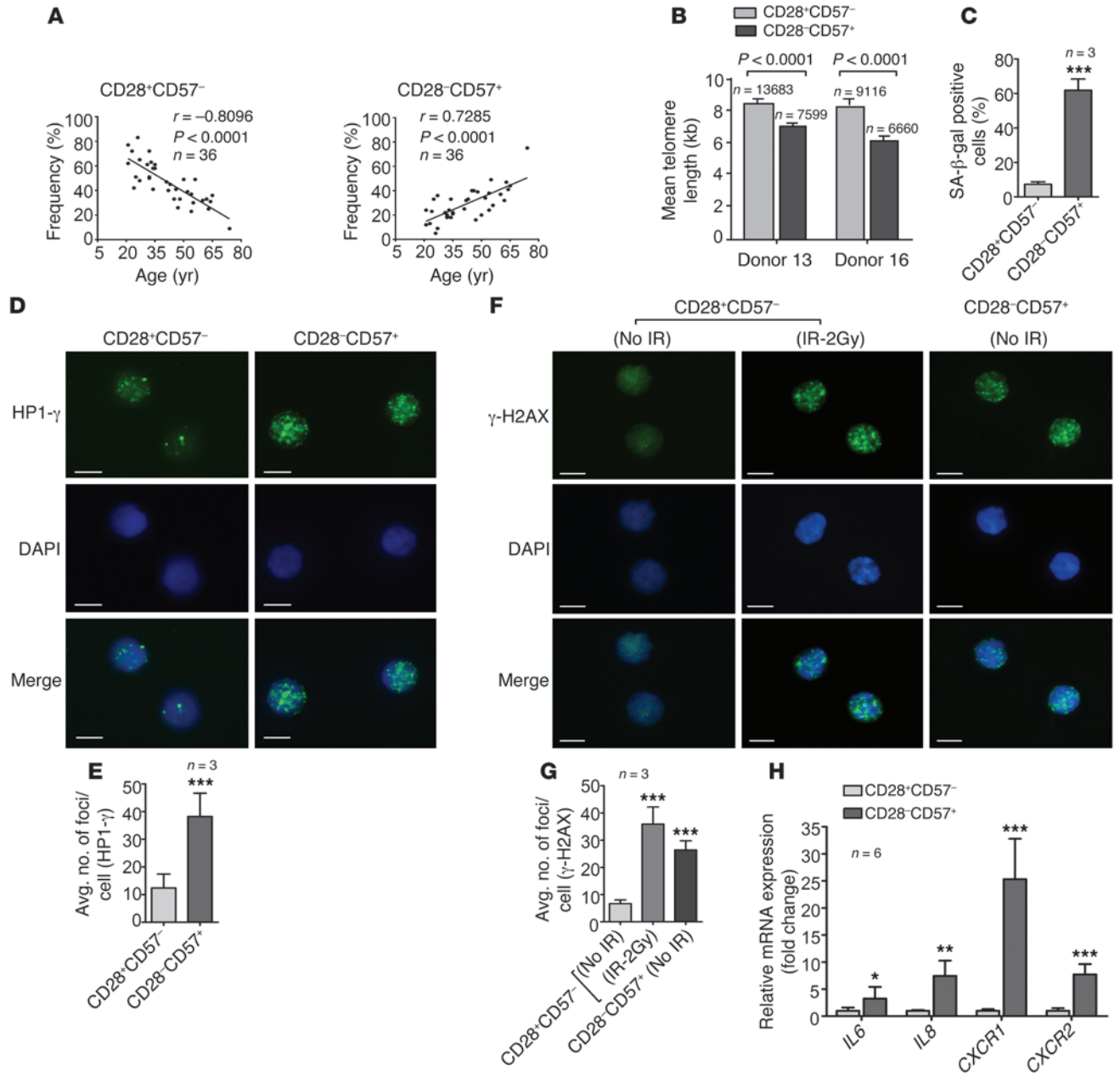

Figure 1

Senescent phenotypes in CD28⁻CD57⁺ subsets of CD8⁺ T lymphocytes in vivo. (**A**) CD28⁺CD57⁻ subsets decreased and CD28⁻CD57⁺ subsets increased with donor age. (**B**) High-throughput quantitative FISH revealed shortened telomeres in CD28⁻CD57⁺ subsets. *n* represents total number of telomere spots analyzed per subset. (**C**) Summary of SA-β-gal activity (donors 4, 6, and 7). (**D**) Representative images for HP1-γ foci by immunofluorescence staining (donor 4). (**E**) Quantitative analysis of HP1-γ foci per cell (donors 4, 6, and 7). (**F**) Representative images for γ-H2AX foci (donor 26). Irradiated (2 Gy) CD28⁺CD57⁻ cells were used as a positive control. IR, irradiation. (**G**) Summary of γ-H2AX foci per cell (donors 26–28). (**H**) Quantitative RT-PCR analysis for SASP factors (donors 1–6). *B2M* was used for normalization. Data are mean ± SEM (**B**) or mean ± SD (**C**, **E**, **G**, and **H**). Scale bars: 5 μm (**D** and **F**). **P* < 0.05; ***P* < 0.01; ****P* < 0.001.

naive T cells (most proliferative and least differentiated) to central memory, effector memory, and effector (least proliferative and terminally differentiated) T cells. Repeated or chronic antigen stimulation throughout the normal lifespan or under pathological conditions (e.g., patients with HIV infection, autoimmune diseases, and cancer; refs. 18–20) drives progression of these differentiation states and results in a large population of late-differentiated CD8⁺ T lymphocytes that are approaching or have reached replicative senescence (21). These cells are characterized by loss of CD28 (a costimulatory receptor; ref. 20) and gain of CD57 (also known as human natural killer–1; ref. 22), as well as shortened telomeres (23), and directly contribute to immunosenescence (20, 24). CD8⁺ T lymphocytes with these characteristics can also be a cause of functional impairment of tumor-specific T cell immunity (25).

Our present study shows for the first time that in vivo accumulation of senescent CD8$^+$ T lymphocytes in blood during physiological aging and in the tumor microenvironment involves changes in endogenous expression of Δ133p53 and p53β, and that manipulated expression of these p53 isoforms can control proliferation and senescent phenotypes of blood CD8$^+$ T lymphocytes.

Results

In vivo accumulation of senescent CD8$^+$ T lymphocytes during physiological aging. Multiparameter flow cytometric analysis of circulating CD8$^+$ T lymphocytes isolated from 36 healthy donors (age, 21–74 years) showed decreased frequency of the CD28$^+$CD57$^-$ subset ($r = -0.8096$; $P < 0.0001$) and increased frequency of the CD28$^-$CD57$^+$ subset ($r = 0.7285$; $P < 0.0001$) with advancing age (Figure 1A, Supplemental Figure 1A, and Supplemental Table 1; supplemental material available online with this article; doi:10.1172/JCI70355DS1), while no or weaker association was found in the CD28$^+$CD57$^+$ ($r = -0.0953$; $P = 0.7883$) or CD28$^-$CD57$^-$ ($r = 0.3934$; $P = 0.0019$) subsets (Supplemental Figure 1B). Consistently, when CD28 and CD57 were separately analyzed, CD8$^+$ T lymphocytes tended to lose CD28 ($r = -0.8224$; $P < 0.0001$) and gain CD57 ($r = 0.5813$; $P < 0.0001$) expression as a function of donor age (Supplemental Figure 1C and refs. 20, 22).

Fluorescence-activated cell sorting (FACS)-sorted individual CD28/CD57 quadrants were examined for cell proliferation by a CFSE proliferation assay (Supplemental Figure 2A). The CD28$^+$CD57$^-$ subset, which decreased with age, showed the highest proliferation rate (proliferation index, 2.61 ± 0.23), while the CD28$^-$CD57$^+$ subset, which increased with age, showed the lowest (proliferation index, 1.19 ± 0.09) (Supplemental Figure 2B). As previously reported for replicatively senescent CD8$^+$ T lymphocytes (23, 26, 27), the CD28$^-$CD57$^+$ subset had shortened telomeres and showed an increase in cells positive for senescence-associated β-galactosidase (SA-β-gal) compared with the CD28$^+$CD57$^-$ subset (Figure 1, B and C, and Supplemental Figure 3). Other senescence markers previously used with other cell types, including formation of HP1-γ foci (28, 29), spontaneous induction of γ-H2AX foci (30), and mRNA expression of SASP factors, such as *IL6*, *IL8*, *CXCR1*, and *CXCR2* (8), were also increased in the CD28$^-$CD57$^+$ subset (Figure 1, D–H, Supplemental Figure 4, and Supplemental Figure 5, A–D). These results indicate that the CD28$^-$CD57$^+$ subsets within CD8$^+$ T lymphocytes, which accumulate in vivo during physiological aging in humans, are characterized by the senescent phenotypes.

Reduced Δ133p53 and elevated p53β expression in senescent CD8$^+$ blood T lymphocytes in vivo. Endogenous protein expression of Δ133p53 and p53β was examined in FACS-sorted CD28/CD57 quadrants of CD8$^+$ blood T lymphocytes using MAP4 (Supplemental Figure 6A and refs. 14, 15) and TLQi9 (14, 15) antibodies, respectively (Figure 2A; see complete unedited blots in the supplemental material). In donors 1 and 2, in which all 4 quadrants were examined, Δ133p53 expression was decreased from the CD28$^+$CD57$^-$ (most proliferative) subset to the CD28$^+$CD57$^+$, CD28$^-$CD57$^-$, and CD28$^-$CD57$^+$ (senescent) subsets (Figure 2A). In all 6 donors examined, the expression level of Δ133p53 in the CD28$^-$CD57$^+$ subset was 1%–22% (average, 10%) of that in the CD28$^+$CD57$^-$ subset ($P < 0.0001$; Figure 2, A and B). The expression level of p53FL was not significantly different between CD28$^+$CD57$^-$ and CD28$^-$CD57$^+$ subsets (Supplemental Figure 7). In contrast, the expression level of p53β in the CD28$^-$CD57$^+$ subset was 1.23- to 2.06-fold (average, 1.72-fold) higher than that in the CD28$^+$CD57$^-$ subset ($P = 0.0020$; Figure 2, A and B). These results were confirmed by immunoblot analysis using a full blot, which was probed with the Δ133p53-specific antibody MAP4 or the antibody CM1 (31), which recognizes p53FL, Δ133p53, p53β, and other p53 isoforms (Supplemental Figure 6, B and C). The elevated levels of p53β protein in the senescent CD28$^-$CD57$^+$ subsets were associated with increased *p53*β mRNA levels (Figure 2C and Supplemental Figure 5E). *SRSF3*, a splicing factor that restricts the alternative splicing generating p53β (16), was downregulated in the CD28$^-$CD57$^+$ subsets (Figure 2D and Supplemental Figure 5F), consistent with the increased *p53*β mRNA (Figure 2C). In contrast, the decreased levels of Δ133p53 protein in the CD28$^-$CD57$^+$ subsets were not associated with a decrease in Δ*133p53* mRNA (Figure 2E and Supplemental Figure 5G), indicative of Δ133p53 downregulation at the protein level in this senescent population of CD8$^+$ T lymphocytes.

To examine a mechanism for the downregulation of Δ133p53 at the protein level, we first used a proteasome inhibitor, MG-132. Whereas treatment with MG-132 resulted in increased p53FL levels in the whole population of CD8$^+$ T lymphocytes and the CD28$^+$CD57$^-$ and CD28$^-$CD57$^+$ populations, the same treatment did not increase Δ133p53 protein levels in any of these populations (Supplemental Figure 8, A and B), which suggests that Δ133p53, unlike p53FL, is not subject to proteasome-mediated protein degradation. We next inhibited autophagy, an alternative mechanism for protein degradation, by treatment with bafilomycin A1 (Figure 2F and Supplemental Figure 8C). This treatment did not stabilize p53FL in either CD28$^+$CD57$^-$ or CD28$^-$CD57$^+$ subsets. While the abundant levels of Δ133p53 in CD28$^+$CD57$^-$ subsets were not affected by this treatment, the reduced levels of Δ133p53 in CD28$^-$CD57$^+$ subsets were upregulated approximately 2- to 3-fold in response to bafilomycin A1 in all 3 cases examined. These results indicate that autophagic degradation of Δ133p53 contributes to its downregulation in senescent CD28$^-$CD57$^+$ subsets of CD8$^+$ T lymphocytes.

Senescence-associated phenotypes and p53 isoform expression profile in tumor-associated CD8$^+$ T lymphocytes. Tumor-associated CD8$^+$ T lymphocytes were isolated from lung cancer tissues of patients who received surgery and were examined for the CD28$^+$CD57$^-$ and CD28$^-$CD57$^+$ subsets. A considerable fraction of CD28$^+$CD57$^-$ (mean, 60.3% ± 12.7%) and CD28$^-$CD57$^+$ (mean, 8.7% ± 6.7%) subsets were observed in the tumor-associated CD8$^+$ T lymphocytes, similar to blood T lymphocytes (Supplemental Tables 1 and 2). The CD28$^-$CD57$^+$ subsets, similar to those from blood CD8$^+$ T lymphocytes, showed switching of p53 isoform abundance, i.e., elevated p53β and diminished Δ133p53 protein levels, and senescence phenotypes, including increased HP1-γ foci and elevated SASP factors, such as *IL6* and *IL8* (Figure 2, G–I, and Supplemental Figure 9, A–D). The elevated levels of p53β protein in the CD28$^-$CD57$^+$ cells were again coincident with increased *p53*β mRNA and decreased *SRSF3* mRNA (Figure 2, J and K, and Supplemental Figure 9, E and F). In contrast, Δ*133p53* mRNA expression was similar in these 2 subsets (Figure 2L and Supplemental Figure 9G), again suggesting regulation at the protein level. These results indicate that CD8$^+$ T lymphocytes in the tumor microenvironment may undergo differentiation and senescence processes similar to those observed in the same cell type in blood during aging.

In vitro replicative senescence of CD8$^+$ T lymphocytes reproduces CD28 loss and diminished Δ133p53 expression observed in vivo. FACS-sorted CD8$^+$ T lymphocytes were stimulated with anti-CD2/3/28 cocktail beads and recombinant human IL-2 (rIL-2) and expanded in culture. The CD8$^+$ T lymphocytes from all 3 donors examined ceased to proliferate after 7–8 weeks and remained quiescent (Figure 3A). In these proliferation-arrested cells, an increase in SA-β-gal–posi-

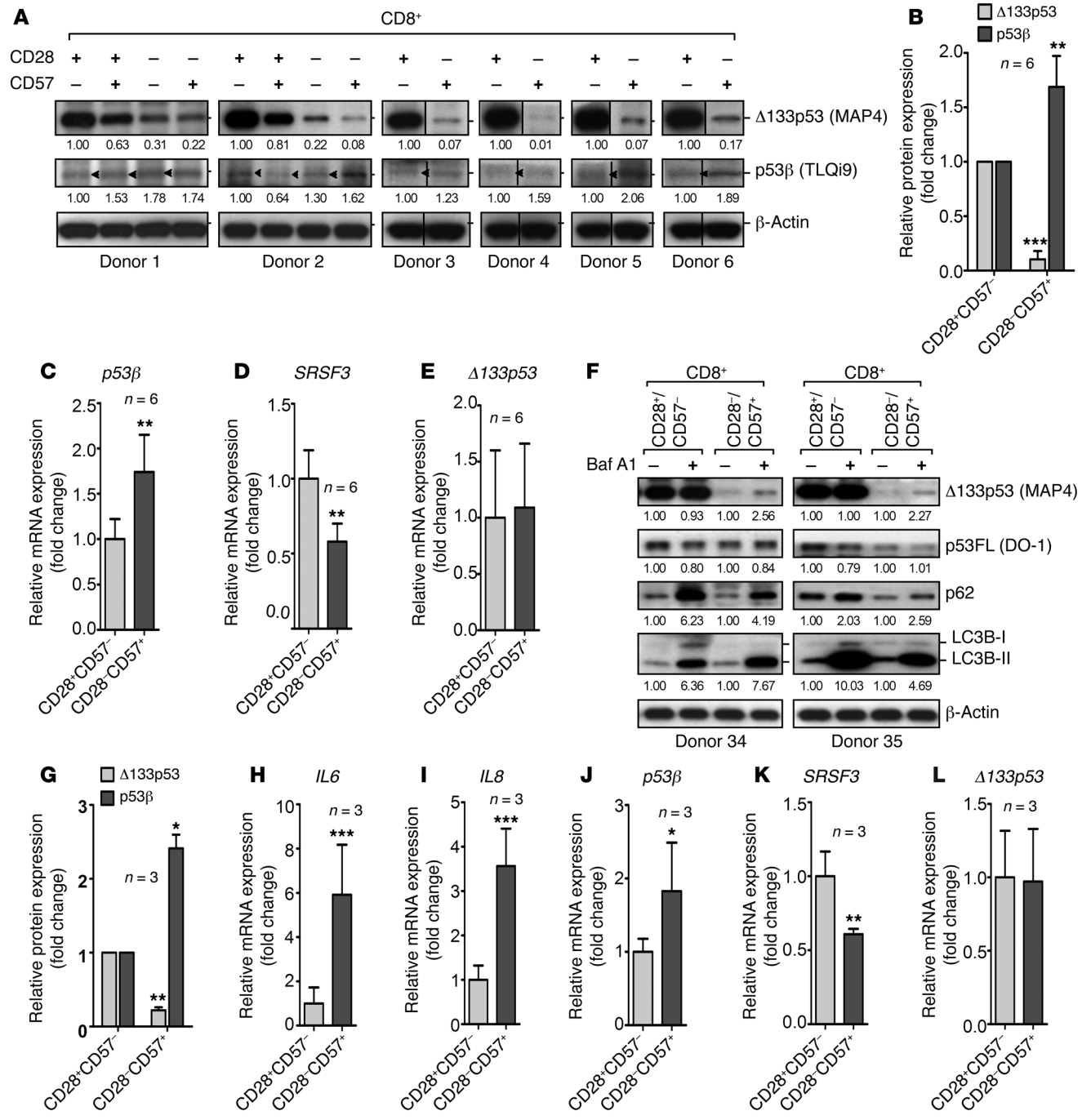

Figure 2

Diminished Δ133p53 and elevated p53β in the CD28⁻CD57⁺ subset of CD8⁺ T lymphocytes in vivo. (**A**) Immunoblot of CD28/CD57 quadrants of blood CD8⁺ T lymphocytes showing Δ133p53 and p53β proteins (donors 1–6). The CD28⁺CD57⁺ and CD28⁻CD57⁻ subsets from donors 3–6 did not give enough amounts of protein because of low cell counts. p53β bands are denoted by thin lines at right of lanes and arrowheads. Lanes were run on the same gel but were noncontiguous (black lines). Densitometric values (normalized to β-actin, expressed relative to the CD28⁺CD57⁻ subset) are shown below. (**B**) Quantitative data summary of Δ133p53 and p53β protein expression (donors 1–6). (**C**–**E**) Quantitative RT-PCR analysis for *p53β* (**C**), *SRSF3* (**D**), and *Δ133p53* (**E**) (donors 1–6). *B2M* was used for normalization. (**F**) Immunoblot of bafilomycin A1–treated (Baf A1; 100 nM for 6 hours) CD28⁺CD57⁻ and CD28⁻CD57⁺ subsets of blood CD8⁺ T lymphocytes (donors 34 and 35). Δ133p53, p53FL (detected by DO-1 antibody), p62, and LC3B proteins were examined. Inhibition of autophagy was confirmed by increased amounts of p62 and LC3B-II. Densitometric values (expressed relative to untreated cells) are shown below. (**G**) Quantitative data summary of Δ133p53 and p53β protein expression in the CD28⁺CD57⁻ and CD28⁻CD57⁺ subsets of tumor-associated CD8⁺ T lymphocytes (tumors 1–3; see Supplemental Figure 9A). (**H**–**L**) Quantitative RT-PCR analysis for *IL6* (**H**), *IL8* (**I**), *p53β* (**J**), *SRSF3* (**K**), and *Δ133p53* (**L**) (tumors 5–7). *B2M* was used for normalization. Data are mean ± SD (**B**–**E** and **G**–**L**). **P* < 0.05; ***P* < 0.01; ****P* < 0.001.

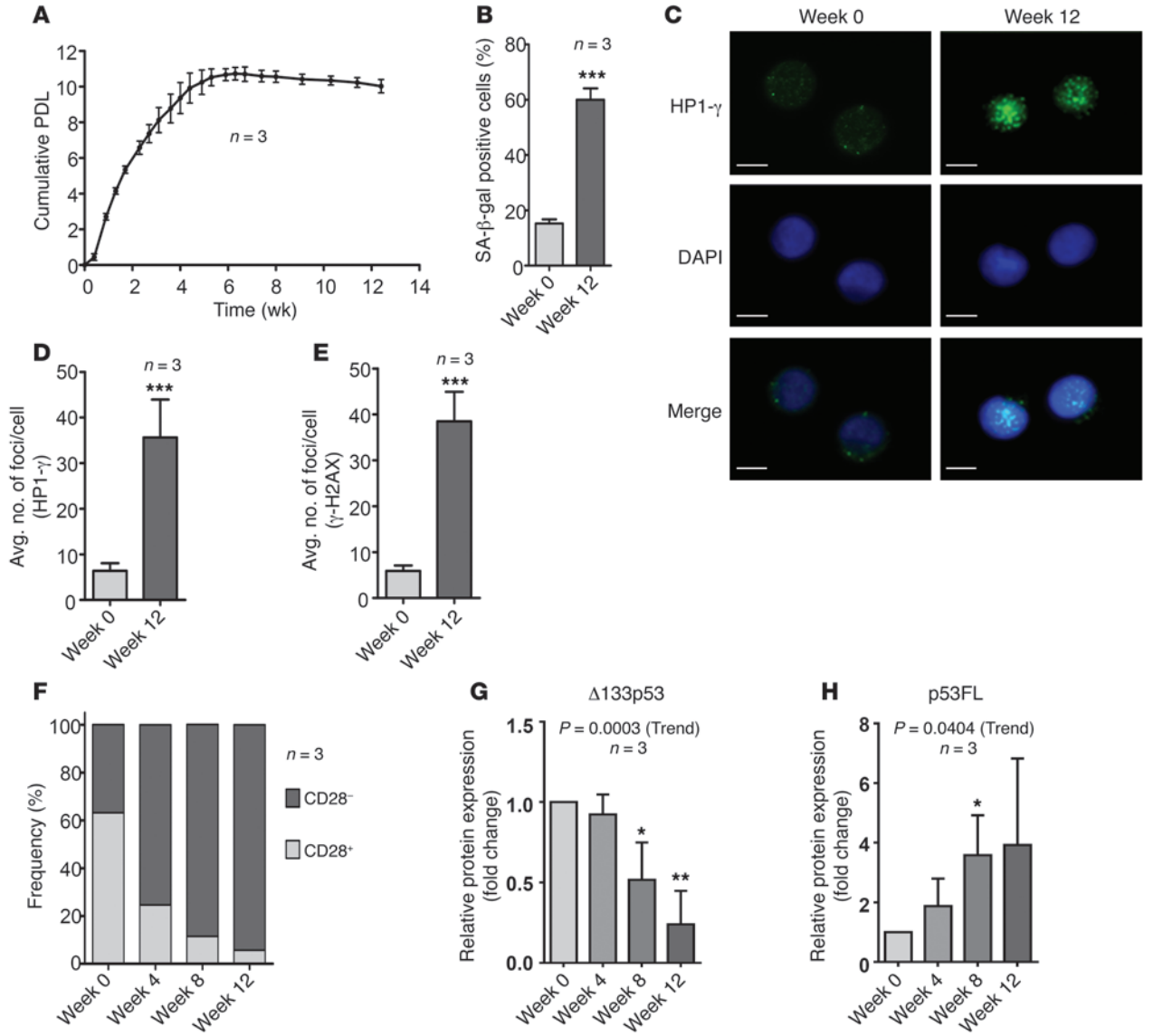

Figure 3

Blood CD8⁺ T lymphocytes undergo replicative senescence in vitro, with loss of CD28 and downregulation of Δ133p53. (**A**) CD8⁺ T lymphocytes after stimulation with anti-CD2/3/28 cocktail and rIL-2 were assessed for cumulative PDLs (donors 29–31). (**B**) Quantitative analysis of SA-β-gal activity (donors 29–31). (**C**) Representative immunofluorescence staining of HP1-γ foci (donor 29). (**D** and **E**) Quantitative analysis of number of HP1-γ (**D**) and γ-H2AX (**E**) foci (donors 29–31). (**F**) Frequency of CD28⁺ and CD28⁻ subsets of the CD8⁺ T lymphocytes during in vitro culture (donors 29–31). (**G** and **H**) Quantitative data summary of Δ133p53 (**G**) and p53FL (**H**) protein expression of the CD8⁺ T lymphocytes during in vitro culture (donors 29–31; see Supplemental Figure 10D). Linear trend analysis was performed, and *P* values are shown. Data are mean ± SD (**A**, **B**, **D**, **E**, **G**, and **H**) or mean values (**F**). Scale bars: 5 μm (**C**). $^*P < 0.05$; $^{**}P < 0.01$; $^{***}P < 0.001$.

tive cells and increased numbers of HP1-γ and γ-H2AX foci were observed (Figure 3, B–E, and Supplemental Figure 10, A and B), similar to the senescent CD8⁺ T lymphocytes that accumulated in vivo (Figure 1, C–G). The frequency of the CD28⁺ population decreased gradually toward the end of the replicative lifespan (week 12; Figure 3F), reproducing its donor age–dependent decrease in vivo, although loss of CD57⁺ population during in vitro culture contradicted the age-dependent increase in CD57⁺ population in vivo (compare Supplemental Figure 1C and Supplemental Figure 10C). All 3 isolates of CD8⁺ T lymphocytes showed a decrease in Δ133p53 expression associated with proliferation arrest at week 8, with or without further decrease at week 12 (Figure 3G and Supplemental Figure 10D). While p53FL was upregulated during in vitro culture, p53β expression showed only a marginal increase or remained constant through week 8 (Figure 3H and Supplemental Figure 10, D–F). These results indicate that CD8⁺ T lymphocytes undergoing replicative senescence in vitro largely recapitulated their aging-associated in vivo phenotypes, including loss of CD28 and diminished expression of Δ133p53, although the lack of increase in CD57 and the undetectable or marginal induction of p53β in vitro may also imply differences between in vivo and in vitro processes of replicative exhaustion of CD8⁺ T lymphocytes.

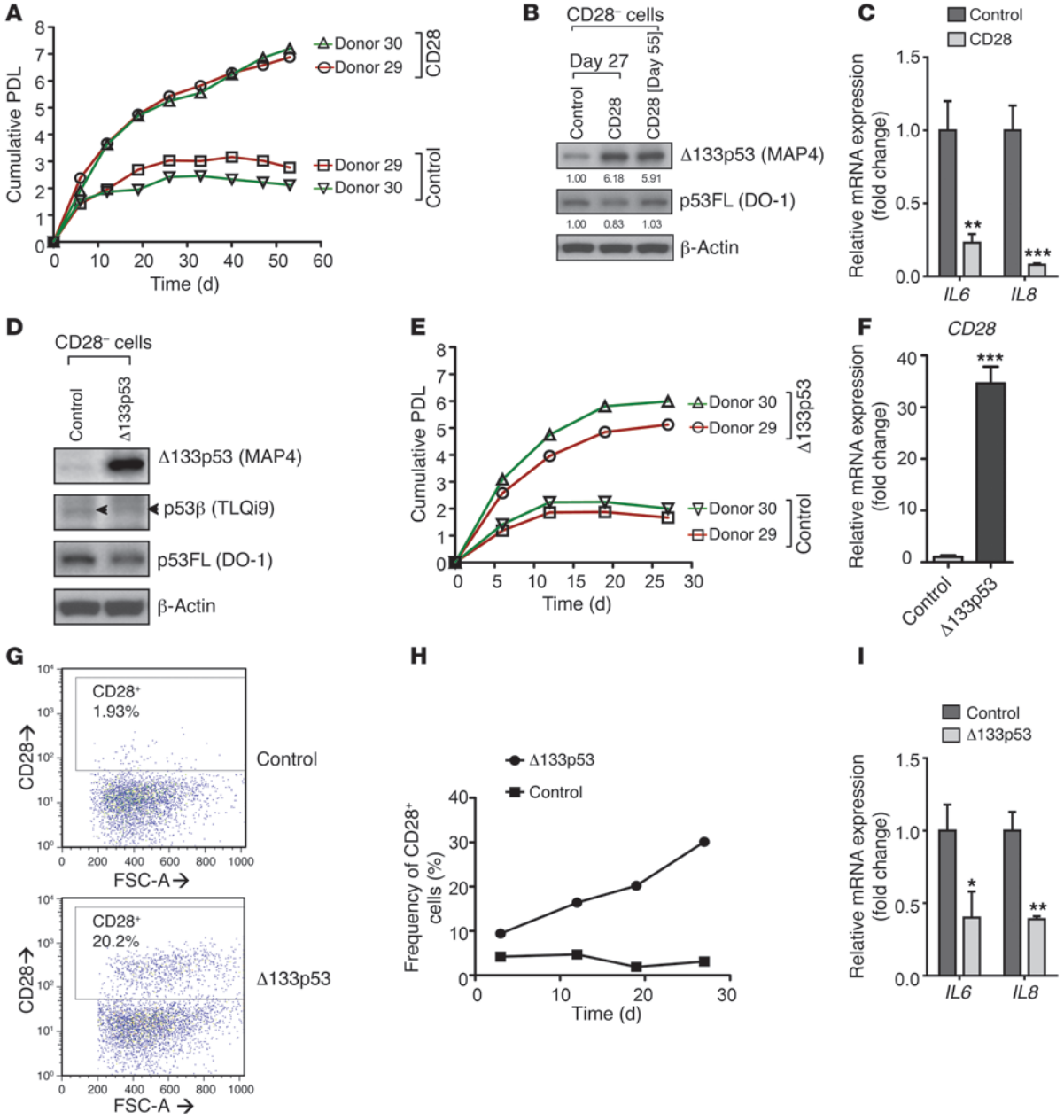

Figure 4

Reconstitution of CD28 or Δ133p53 expression extends replicative lifespan in CD8⁺CD28⁻ T lymphocytes. (**A**) Cumulative PDLs of CD28-reconstituted CD28⁻ cells (donors 29 and 30) after puromycin selection. Empty vector was used as control. (**B**) Immunoblot analysis of Δ133p53 and p53FL (donor 29, days 27 and 55). β-actin was the loading control for normalization. Expression level relative to control is shown below. (**C**) Quantitative RT-PCR analysis for *IL6* and *IL8* in CD28-reconstituted CD28⁻ cells (donors 29 and 30, day 20). *B2M* was used for normalization. (**D**) Reconstitution of Δ133p53 expression in CD28⁻ cells (donor 29). Immunoblot analysis was performed 12 days after blasticidin selection. p53β and p53FL levels were not affected. p53β bands are denoted by arrowheads. (**E**) Cumulative PDLs of Δ133p53-reconstituted CD28⁻ cells after blasticidin selection (donors 29 and 30). Cells with control vector are also shown. (**F**) Quantitative RT-PCR of *CD28* mRNA (donor 29, day 19). *B2M* was used for normalization. (**G**) Representative dot plots for CD28 expression by flow cytometry (donor 29, day 19). (**H**) Frequency of CD28⁺ cells at days 3, 12, 19 (as in **G**), and 27 (donor 29). (**I**) Quantitative RT-PCR analysis for *IL6* and *IL8* in Δ133p53-reconstituted CD28⁻ cells (donors 29 and 30, day 19). *B2M* was used for normalization. Data are mean ± SD (**C**, **F**, and **I**), from triplicate assays (**F**). $^{*}P < 0.05$; $^{**}P < 0.01$; $^{***}P < 0.001$.

Reconstitution of either CD28 or Δ133p53 restores cell proliferation, extends replicative lifespan, and rescues senescence phenotypes in CD8⁺CD28⁻ T lymphocytes. Given that CD28 loss occurs during both in vivo and in vitro replicative senescence, we chose CD8⁺ T lymphocytes sorted based on CD28 expression (CD28⁺ and CD28⁻ populations) as recipient cells in gene transduction experiments to examine the mechanistic role of the p53 isoforms. When CD28⁺ and CD28⁻ populations were compared, the former showed remarkably higher rep-

licative potential than the latter (~14 versus ~5 PDLs; Supplemental Figure 11A), as expected from the CFSE cell proliferation assay (Supplemental Figure 2) and previous reports (32). Compared with $CD28^+$ cells, $CD28^-$ cells expressed decreased Δ133p53 protein and elevated p53β protein levels, again with unchanged Δ*133p53* mRNA, increased *p53*β mRNA, decreased *SRSF3* mRNA, and elevated *IL6* and *IL8* levels (Supplemental Figure 11, B–G), consistent with the results from CD28/CD57 quadrants (Figures 1 and 2).

To examine the functions of CD28 and Δ133p53 in blood $CD8^+$ T lymphocytes, we reconstituted their expression in Δ133p53-low $CD8^+CD28^-$ cells (Figure 4). When CD28 expression was reconstituted by transducing a CD28 retroviral expression vector (Supplemental Figure 12, A and B), the cells reproducibly had an extended replicative lifespan by more than 4 PDLs compared with vector-transduced control cells (Figure 4A), in agreement with a previous report using whole $CD8^+$ T lymphocytes (17). Reconstitution of CD28 restored the expression of Δ133p53 protein without changes in Δ*133p53* mRNA levels, p53FL levels, or $CD57^+$ cell frequency (Figure 4B and Supplemental Figure 12, C–E). These CD28-reconstituted $CD28^-$ cells also showed decreased expression of *IL6* and *IL8* (Figure 4C). When $CD28^-$ cells were transduced with a lentiviral construct for Δ133p53 expression (Figure 4D), the transduced cells showed higher proliferation rate, bypassed the senescence point of vector control cells, and continued to proliferate for 4 or 5 more PDLs (Figure 4E). A similar extension of replicative lifespan was also observed when Δ133p53 was overexpressed in whole $CD8^+$ cells (Supplemental Figure 13, A and B). Upon Δ133p53 expression in $CD28^-$ cells, *CD28* mRNA expression was induced, and up to 30% of cells were converted to $CD28^+$ (Figure 4, F–H), whereas CD57 expression was unaltered (Supplemental Figure 14, A and B). Expression of *IL6* and *IL8* was reduced in Δ133p53-rescued $CD28^-$ cells (Figure 4I), similar to the CD28-rescued cells (Figure 4C). In addition to the attenuation of senescence factors, these Δ133p53-rescued $CD28^-$ cells also showed increased expression of central memory markers like CD27 and CD62L and decreased expression of late-differentiated markers like PD-1 and LAG-3 (Supplemental Figure 14, C–J). These findings indicate that Δ133p53, through upregulation of the costimulatory receptor CD28, plays a physiological role in regulating $CD8^+$ T lymphocyte proliferation, senescence, and function.

Since Δ133p53 dominant-negatively inhibits the transcriptional activity of p53FL for p53 target genes, including p53-repressed genes (15), and *CD28* contains a p53 response element within its intron 1 (p53FamTag; http://p53famtag.ba.itb.cnr.it/), we hypothesized that the transcriptional repression of *CD28* by p53FL is a mechanistic basis for the Δ133p53-induced upregulation of *CD28* at the mRNA level. In whole $CD8^+$ T lymphocytes from 3 donors, treatment with nutlin-3a (an inhibitor of MDM2), but not nutlin-3b (an inactive enantiomer), resulted in the activation of p53FL, evidenced by increased amounts of p53FL protein, increased p53 phosphorylation at the serine 15 residue, and induced expression of a p53 target, $p21^{WAF1}$ (Supplemental Figure 15A). Under this condition, $CD28^+$ cell frequency was decreased, which was attributed to decreased expression of *CD28* mRNA (Supplemental Figure 15, B–D). To examine the effect of Δ133p53 on the p53FL-mediated repression of *CD28*, Δ133p53 was overexpressed in whole $CD8^+$ T lymphocytes. While nutlin-3a treatment in control vector–transduced cells resulted in significant repression of *CD28* mRNA (60% decrease), similar to that observed in untransduced cells, Δ133p53 overexpression largely abrogated the repressive effect of nutlin-3a on *CD28* mRNA expression (19% decrease) (Supplemental Figure 15, D and E). These results suggest that Δ133p53 counteracts the p53FL-mediated transcriptional repression of *CD28*.

Knockdown of Δ133p53 or overexpression of p53β induces cellular senescence in $CD8^+CD28^+$ T lymphocytes. Highly proliferative $CD28^+$ populations with abundant levels of Δ133p53 (Supplemental Figure 11, A and B) were used in a further mechanistic experiment, in which endogenous Δ133p53 expression was knocked down. A siRNA oligonucleotide against Δ133p53, which was transfected every 3–4 days by nucleofection, efficiently downregulated Δ133p53 expression with no effect on p53FL (Figure 5A). The cells with Δ133p53 knockdown underwent proliferation arrest within 10 days of induction of SA-β-gal activity, whereas control cells were proliferating well (Figure 5, B and C, and Supplemental Figure 16A). Knockdown of Δ133p53 decreased *CD28* mRNA expression and $CD28^+$ cell number, with no remarkable change in $CD57^+$ cells (Figure 5, D and E, and Supplemental Figure 16, B–D), again indicating that Δ133p53 positively regulates *CD28* at the mRNA level.

Upregulation of endogenous p53β during in vivo senescence (Figure 2A) was mimicked in vitro by lentiviral overexpression of Flag-tagged p53β in the $CD28^+$ population (Figure 5F), which were p53β-low (Supplemental Figure 11B). While vector control cells were proliferating well, the p53β-overexpressing cells stopped proliferating after 10 days, with an increase in SA-β-gal activity (Figure 5, G and H, and Supplemental Figure 17A), similar to the results using whole $CD8^+$ T lymphocytes (Supplemental Figure 13). Overexpression of p53β was associated with a significant increase in $CD57^+$ cells, but not $CD28^+$ cells (Supplemental Figure 17, B–E), suggesting coregulation of p53β and CD57. *IL6* and *IL8* were consistently upregulated in the p53β-overexpressing senescent $CD28^+$ cells (Figure 5I). Conversely, PD-1 and LAG-3 were reproducibly upregulated in the senescent $CD28^+$ cells overexpressing p53β (Figure 5, J and K, and Supplemental Figure 17, F and G). These findings suggest that p53β overexpression leads cells toward senescence, with expression of senescence-associated factors as well as terminally differentiated markers such as PD-1 and LAG-3.

Discussion

In this study of $CD8^+$ T lymphocytes from healthy human donors, we observed age-dependent in vivo accumulation of late-differentiated cells, which were associated with specific changes in cell surface antigens (loss of CD28 and gain of CD57) (20, 22), as well as various senescence markers and phenotypes, such as SA-β-gal activity, shortened telomeres (23, 33), poor proliferation (21, 34), increased HP1-γ foci (29), increased γ-H2AX foci (35), and increased SASPs (8). In these physiologically senescent or near-senescent $CD8^+$ T lymphocytes, Δ133p53 expression was diminished and p53β expression was increased, similar to our previous observations with senescent human fibroblasts in vitro and pathologically induced in vivo senescence in premalignant tumors (15). The $CD28^-CD57^+$ populations of tumor-associated $CD8^+$ T lymphocytes from lung cancer tissues also showed downregulation of Δ133p53 and upregulation of p53β. The regulatory mechanisms for the p53 isoform expression may be conserved in $CD8^+$ T lymphocytes (present study) and fibroblasts (15). p53β is likely to be regulated by SRSF3-mediated alternative splicing in both cell types (16), and the change in Δ133p53 occurs at the protein level, but not the mRNA level, in both cell types. There is unlikely to be a direct relationship between the regulation of p53β and Δ133p53 expression, because overexpression of either one did not affect the expression level of the other (Figure 4D and Figure 5F).

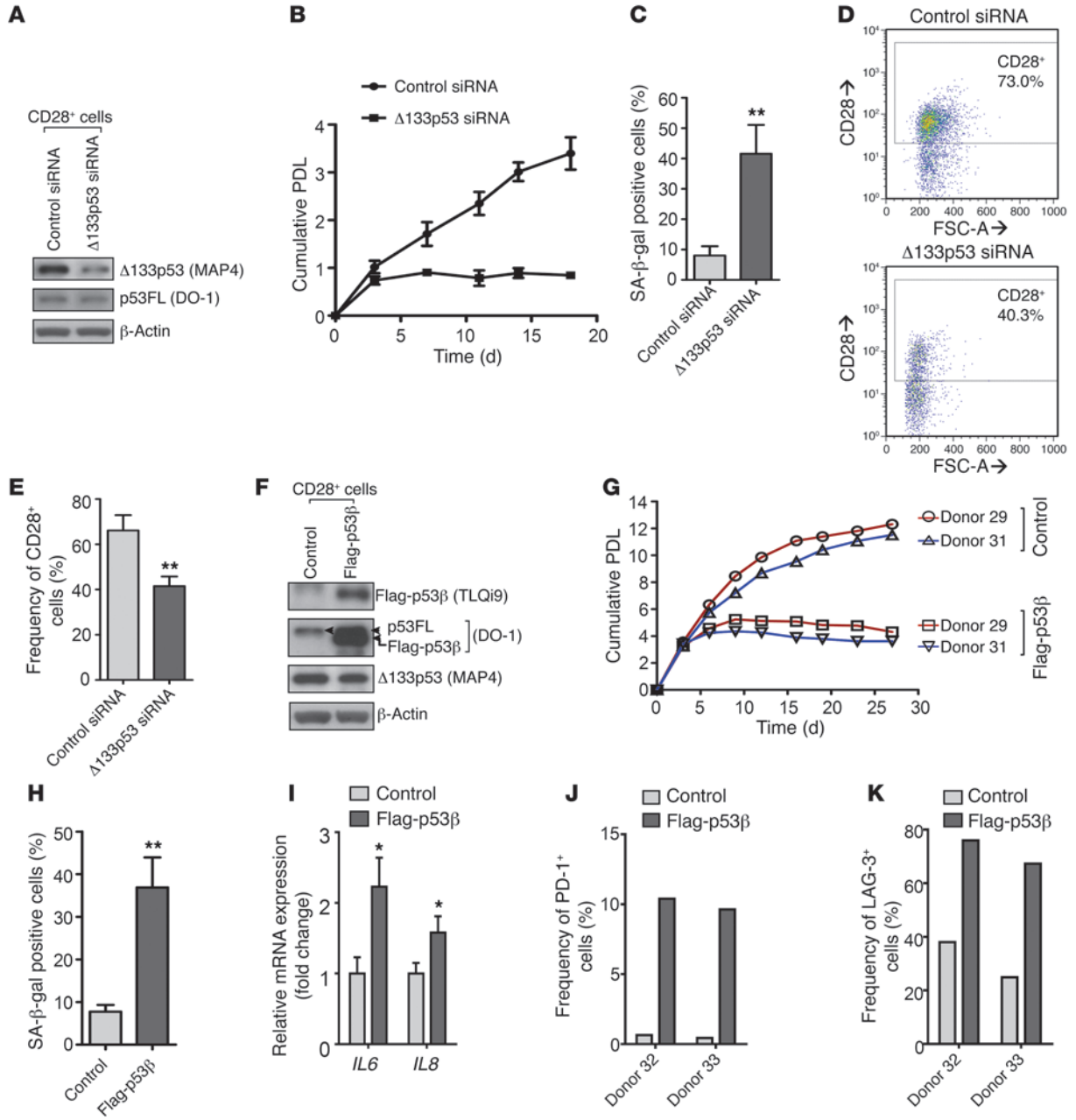

Figure 5

Δ133p53 knockdown or p53β overexpression induces cellular senescence in CD8+CD28+ T lymphocytes. (**A**) Δ133p53 siRNA– or control siRNA–nucleofected CD28+ cells were analyzed by immunoblot analysis of Δ133p53 and p53FL (donor 30, day 7). (**B**) Nucleofections were performed every 3–4 days, 5 consecutive times. Cumulative PDLs were plotted against days after the first nucleofection (donors 29–31). (**C**) Quantitative analysis of SA-β-gal activity (donors 29–31, day 18). (**D**) Representative dot plots for CD28 expression by flow cytometry (donor 30, day 18). (**E**) Quantitative analysis of CD28+ cells (donors 29–31, day 18). (**F**) Flag-tagged p53β- or control vector–transduced CD28+ cells were analyzed by immunoblot analysis of the indicated proteins after FACS sorting based on vector-derived GFP expression (donor 29, day 7). Overexpression of Flag-p53β was confirmed by TLQi9 and DO-1 antibodies. Δ133p53 was not substantially affected. (**G**) Cumulative PDLs of Flag-p53β–overexpressing CD28+ cells (donors 29 and 31). Cells with control vector are also shown. (**H**) Quantitative analysis of SA-β-gal activity (donor 29, day 19). (**I**) Quantitative RT-PCR analysis for *IL6* and *IL8* in p53β-reconstituted CD28+ cells (donors 29 and 31, day 19). *B2M* was used for normalization. (**J** and **K**) Frequency of PD-1+ (**J**) and LAG-3+ (**K**) cells (donors 32 and 33, day 19). Data are mean ± SD (**B**, **C**, **E**, **H**, and **I**), from triplicate assays (**H**). **P* < 0.05; ***P* < 0.01.

Successive in vitro culture of isolated CD8+ T lymphocytes from blood resulted in senescent proliferation arrest with CD28 loss and Δ133p53 downregulation, consistent with their regulation during in vivo aging, enabling in vitro functional analyses of the costimulatory receptor and the p53 isoforms. The ability of Δ133p53 to extend replicative lifespan was shown in CD8+ T lymphocytes from blood. When Δ133p53 expression was restored in the Δ133p53-low CD28− population that corresponded to cells undergoing or

approaching senescence (20, 21), Δ133p53 delayed the onset of senescent proliferation arrest, extended the replicative lifespan, and rescued cells from senescence phenotypes as efficiently as the reconstitution of CD28. The extension of the replicative lifespan by Δ133p53 restoration was coincident with restored expression of CD28 along with CD27 and CD62L, suggestive of a functional conversion to a less-differentiated, more-proliferative state, such as that of central memory T cells (25). When the in vivo senescence-associated changes in the p53 isoform expression (i.e., p53β upregulation and Δ133p53 downregulation) were reproduced by p53β overexpression or Δ133p53 knockdown, cellular senescence was induced in an otherwise highly proliferative $CD28^+$ population, further validating the physiological roles of the p53 isoforms in regulating proliferation and senescence of $CD8^+$ T lymphocytes.

Our data provide a mechanistic basis for the regulatory interaction between CD28 and Δ133p53, which mutually upregulate the expression of each other. The autophagic degradation of Δ133p53 is in contrast to the proteasome-mediated degradation of p53FL and p53β (15), thus leading to the isoform-specific expression profile of Δ133p53. This finding links CD28 function to Δ133p53 upregulation at the protein level, since NF-κB and its activation of mTOR, a major downstream pathway activated by the CD28 signaling, may repress autophagy (36–40). Our data also suggest that an additional mechanism may exist for the CD28-mediated regulation of Δ133p53, in that the bafilomycin A1 only partially restored Δ133p53 protein levels in $CD28^-CD57^+$ subsets compared with the levels in $CD28^+CD57^-$ subsets (Figure 2F and Supplemental Figure 8C). We showed that the activation of p53FL repressed *CD28* mRNA expression, which was abrogated by Δ133p53 overexpression. Together with our previous finding that Δ133p53 functions as a dominant-negative inhibitor of p53FL (15), these data suggest a mechanism by which Δ133p53, which lacks the transactivation domain (14), transcriptionally activates *CD28* mRNA expression.

Tumor-associated $CD8^+$ T lymphocytes may undergo differentiation and senescence in response to chronic exposure to tumor antigens, as blood $CD8^+$ T lymphocytes respond to chronic infectious agents. In addition, cross-talk between these T lymphocytes and tumor cells likely exists in the tumor microenvironment. Tumor-induced senescence of T lymphocytes is also mediated by tumor-derived soluble factors (41). Senescent $CD8^+$ T lymphocytes not only contribute to tumor immune evasion through their functional unresponsiveness (42) and their suppressor function toward responder T cells (41, 43), but may also actively promote tumor progression through SASP factors such as *IL6* and *IL8*. The senescence-associated change in Δ133p53 and p53β expression in tumor-associated $CD8^+$ T lymphocytes, together with the similar change in premalignant tumors and its reversion during malignant progression in our previous study (15), suggests that these p53 isoforms regulate tumorigenesis in vivo in both tumor cell–autonomous and non-autonomous manners.

This study not only improves understanding of the regulation of $CD8^+$ T lymphocytes, but may also suggest a strategy to overcome immunosenescence. Restoration of cell proliferation and function in terminally differentiated or senescent $CD8^+$ T lymphocytes in blood could reinstate systemic cell-mediated immunity in the elderly and patients with chronic antigen exposure (e.g., patients with HIV) (18, 19, 44, 45). Tumor-specific, tumor-infiltrating $CD8^+$ T lymphocytes that are terminally differentiated or senescent could be functionally restored for adoptive cell transfer therapies against cancer (25). The Δ133p53-induced restoration of the costimulatory receptor CD28 and the central memory markers CD27 and CD62L, as well as the attenuation of the terminal differentiation markers PD-1 and LAG-3, suggests that enhanced expression of Δ133p53 may be a strategy for dedifferentiating and expanding $CD8^+$ T lymphocytes toward future clinical applications. Of particular relevance is that the blockade of PD-1 and its ligand has recently emerged as a novel, promising immunotherapy against lung cancer and other cancers (46, 47).

A growing body of evidence, including the present study and a prior report of reprogramming of senescent human fibroblasts into induced pluripotent stem cells (iPSCs; ref. 48), suggests that near-senescent or senescent cells can be induced back into a proliferative state. Recently, iPSCs were derived from human $CD8^+$ T lymphocytes (49). Direct reprogramming or iPSC reprogramming and subsequent redifferentiation may convert terminally differentiated cells to naive or early-differentiated states (50). However, these methods usually involve an oncogenic factor such as c-Myc or SV40 large T antigen (49, 51–53). Since Δ133p53 is a natural isoform of p53 and is physiologically expressed in normal proliferative cells at high levels, enhanced expression of Δ133p53 may lead to a safe method for functional restoration of $CD8^+$ T lymphocytes with minimum concern for malignant transformation.

Methods

Cell cultures and reagents. Mononuclear cells from blood or single-cell dissociated lung tumors (54) were obtained by density gradient centrifugation with Histopaque-1077 (Sigma-Aldrich) and then used for flow cytometric staining or stored in liquid N_2 with freezing media (Invitrogen) until use. $CD8^+$ T lymphocytes and their $CD28^+$ and $CD28^-$ subsets were isolated from PBMCs using FACS or by magnetic bead–activated cell sorting (MACS) using the EasySep CD8 enrichment kit (Stemcell). The CD28/CD57 quadrants ($CD28^+CD57^-$, $CD28^+CD57^+$, $CD28^-CD57^-$, and $CD28^-CD57^+$) of $CD8^+$ T lymphocytes were isolated by FACS. Cell cultures were established as described previously (17, 55, 56). Briefly, cells were cultured at 1×10^6/ml in AIM-V complete medium (Invitrogen) supplemented with 300 IU/ml rIL-2 (PeproTech) and 5% heat-inactivated human AB serum (Valley Biomedical) unless otherwise specified. RPMI-1640 complete medium (Invitrogen) supplemented with 10% fetal bovine serum (Gibco), 10 mM HEPES (Invitrogen), 2 mM glutamine (Invitrogen), 50 IU/ml penicillin/streptomycin (Invitrogen), and 20 IU/ml rIL-2 was used in Supplemental Figure 2. Stimulation was either with 1 μg/ml phytohemagglutinin-L (PHA-L; Sigma-Aldrich) for 48 hours or with anti-CD2/3/28 microbead cocktail (Miltenyi Biotec) for 72 hours. Cell viability was determined by trypan blue exclusion every 3–4 days, and when the cell density reached $\geq 2 \times 10^6$/ml, cells were subcultured at 1×10^6/ml. Population doubling levels (PDLs) were calculated as $\log_{10}$(number of cells counted after expansion) – $\log_{10}$(number of cells seeded)/$\log_{10}2$. Bafilomycin A1 and MG-132 were from Sigma-Aldrich. Nutlin-3b and nutlin-3a were from Cayman Chemical Company.

Flow cytometry and cell sorting. Mononuclear cells were washed with cold PBS plus 0.5% BSA or with RPMI-1640 complete medium and incubated with FcR blocking reagent (Miltenyi Biotec) for 15 minutes at 4°C. Cells were then stained with APC-Cy7– or FITC-conjugated anti-human CD8 (BD Biosciences), APC-conjugated anti-human CD28 (BD Biosciences), PE-conjugated anti-human CD57 (Abcam), PE-Cy7–conjugated anti-human CD27 (BD Biosciences), APC-conjugated anti-human CD62L (BD Biosciences), PE-conjugated anti-human PD-1 (BD Biosciences), and FITC-conjugated anti-human LAG-3 (LifeSpan Biosciences) for 30 minutes on ice. 7-AAD (BD Biosciences) was used to assess the viability of cells. Fluorescence data from at least 10,000 cells were acquired using FACSDiva software in LSRII (BD Biosciences). Data were analyzed using FlowJo (Tree Star Inc.). The purity of each population was checked and >90% pure cells were used for all experiments.

Proliferation assay. Cells were stained with CFSE using the Vybrant CFDA SE Cell Tracer kit (Invitrogen) as described previously (57). CFSE-stained cells were washed twice with RPMI-1640 complete medium before they were cultured at 1×10^6 cells/ml. Stimulation was performed with PHA-L at day 0. Cells were immunostained with anti-CD8–APC-Cy7, anti-CD28–APC, and anti-CD57–PE at day 5, and fluorescence data were acquired as described above. The proliferation index was calculated from the data (total number of cell divisions that took place/number of cells that went into division) using FlowJo (Tree Star Inc.).

Immunoblot analysis. Cells were lysed in RIPA buffer or RIPA buffer with phosphatase inhibitor and immunoblotted as described previously (14, 15). Primary antibodies used were as follows: MAP4 (1:7,500; a polyclonal antibody raised in rabbit with a mixture of peptides MFCQLAKTC and FCQLAKTCP corresponding to the N terminus of human Δ133p53 protein; refs. 14, 15) for Δ133p53; TLQi9 (1:5,000; a polyclonal antibody raised in rabbit using peptide TLQDQTSFQKENC corresponding to the C terminus of human p53β protein; ref. 14) for p53β; DO-1 (1:2,000; Santa Cruz Biotechnology) and CM1 (1:1,000; ref. 14) for p53FL; M2 monoclonal antibody (1:10,000; Sigma-Aldrich) for FLAG tag; AC-15 (1:10,000; Sigma-Aldrich) for β-actin; anti–γ-H2AX (1:1,000; Cell Signaling); P-p53^{S15} (1:1,000; Cell Signaling) for phosphorylated p53; anti-p21^{WAF1} (1:500; CalBiochem); anti-p62/SQSTM1 (1:3,000; MBL); anti-LC3B (1:1,000; Cell Signaling). Horseradish peroxidase–conjugated goat anti-mouse (1:5,000) or anti-rabbit (1:5,000) antibodies (Santa Cruz Biotechnology) were used as secondary antibodies. Signals were detected according to standard procedures using ECL detection (Amersham Biosciences) or SuperSignal West Dura Extended Duration system (Pierce Biotechnology). Quantitative analysis of the immunoblot data was performed using ImageJ 1.42q software (http://rsb.info.nih.gov/ij/).

Immunocytochemistry. Cultured cells or FACS-sorted subsets were immunostained for HP1-γ and γ-H2AX using a standard protocol. Briefly, cells were fixed with 4% PFA in PBS for 15 minutes on ice followed by permeabilization using PBS with 0.5% BSA and 0.05% Triton-X-100 on ice for 10 minutes. Cells were blocked for 1 hour with 10% donkey serum in PBS on ice, then incubated for 1 hour on ice with rabbit polyclonal anti–HP1-γ (1:800; Cell Signaling) or anti–γ-H2AX (1:400; Cell Signaling). Secondary incubation was performed with Alexa Fluor 488–conjugated donkey polyclonal anti-rabbit (1:200; Invitrogen) for 1 hour on ice. Stained cells were transferred onto glass slides (poly-L-lysine coated) using cytospin-3 (Shandon) at 100 *g* for 5 minutes. Immediately after cytospin, the glass slides were mounted with DAPI solution. Digital images were acquired using Openlab 3.1.5 software (Improvision Inc.).

Telomere length analysis. High-throughput quantitative FISH was performed to compare the telomere lengths of the CD28$^+$CD57$^-$ and CD28$^-$CD57$^+$ subsets as described previously (58). The 4′,6-diamidino-2-phenylindole channel was used for nuclear staining and the CY3 for telomere detection. Telomere length values were analyzed using individual telomere spots (>6,000 per sample). Telomere fluorescence values were converted into kb by external calibration with the L5178Y-S and L5178Y-R lymphocyte cell lines with stable and known telomere lengths of 10.2 and 79.7 kb, respectively (59).

SA-β-gal assay. Cytospun cells were examined using the Senescence β-Galactosidase Staining Kit (Cell Signaling) per the manufacturer's instructions.

Lentiviral and retroviral plasmid construct and transduction. Δ133p53 and Flag-p53β cDNAs (15) were cloned into the lentiviral vector pLoc-GFP-blasticidin (Open Biosystem). The lentiviral constructs, together with the TransLentiviral GIPZ packaging system (Open Biosystem), were transfected into 293T/17 cells using Lipofectamine-2000 (Invitrogen), and the viral particles were collected 48 hours after transfection. The pBABE retroviral vectors containing either CD28-puromycin or empty vector–puromycin were provided by R. Effros (UCLA Vectorcore, Los Angeles, California, USA). The retroviral constructs were transfected into Phoenix A packaging cells (Orbigen Inc.) using Lipofectamine 2000 (Invitrogen), and viral supernatants were collected 48 hours after transfection. Viral particles were titrated and concentrated using Lenti-X/Retro-X Concentrator (Clontech). Sorted cells at day 0 were activated with anti-CD2/3/28 microbead cocktail (Miltenyi Biotec). At days 1 and 2, transductions were performed by spinoculation at 1,000 *g*, 32°C, for 2 hours in presence of protamine sulfate (10 μg/ml; Sigma-Aldrich). 6 hours after the second transduction, the medium was replaced with AIM-V complete media. At day 5, transduced cells were selected either by FACS sorting on basis of GFP expression or by using appropriate concentrations of antibiotics: blasticidin (4 μg/ml for 10–12 days; Invitrogen) or puromycin (2 μg/ml for 3 days; Sigma-Aldrich). Transduced gene expression was confirmed to be stable by immunoblot throughout the replicative lifespan of the cells.

siRNA knockdown. Of 2 siRNA oligonucleotides previously shown to specifically knock down Δ133p53 in normal human fibroblasts (15), 133si-2 (5′-CUUGUGCCCUGACUUUCAA[dT][dT]-3′) was used here because it caused more efficient knockdown via nucleofection. The Δ133p53 siRNA oligonucleotide and its scrambled control were synthesized by Invitrogen. The siRNA oligos were nucleofected at a final concentration of 300 nM using P3 Primary Cell 96-well Nucleofector Kit (Lonza). In experiments where cellular replicative lifespan was examined, nucleofection was repeated every 3–4 days, 5 consecutive times.

Real-time qRT-PCR. RNA samples were prepared using TRIzol (Invitrogen). Reverse transcriptase reaction was performed using SuperScript III First Strand Synthesis System (Invitrogen). Taqman Universal PCR Master Mix (Applied Biosystems, catalog no. 4304437) was used with the following probes and primers (all from Applied Biosystems): Δ*133p53* (forward, 5′-ACTCTGTCTCCTTCCTCTTCCTACAG-3′; reverse, 5′-GTGTGGAATCAACCCACAGCT-3′; probe, 5′-TCCCCTGCCCTCAACAAGATGTTTTGCC-3′); *CD28* (Hs01007422_m1); *CD57* (Hs00218629_m1); *IL6* (Hs00174131_m1); *IL8* (Hs00174103_m1); *CXCR1* (Hs00174146_m1); *CXCR2* (Hs01011557_m1). SYBR green PCR Master mix (Applied Biosystems, catalog no. 4367659) was used for *p53*β (forward, 5′-CTTTGAGGTGCGTGTTTGTGC-3′; reverse, 5′-TTGAAAGCTGGTCTGGTCCTGA-3′; ref. 16) and *SRSF3* (forward, 5′-AGCTGATGCAGTCCGAGAG-3′; reverse, 5′-GGTGGGCCACGATTTCTAC-3′; ref. 16) primers. The internal control was *B2M* (Applied Biosystems, catalog no. 4326319E). Normalized expression was calculated using the ΔΔCt method according to the supplier's protocol (Applied Biosystems, protocol no. 4310255B, user bulletin no. 4303859B).

Statistics. Unless otherwise indicated, statistical analyses were carried out using 2-tailed Student's *t* test for paired and unpaired samples as appropriate. A *P* value less than 0.05 was considered significant.

Study approval. Human peripheral blood samples were collected from healthy donors after informed consent and in accordance with the NIH IRB (study no. 99-CC-0168). Lung tumors were obtained through the CINJ Biospecimen Repository Services under UMDNJ IRB approval (study no. 0220100267).

Acknowledgments

We thank Rita Effros and Mark E. Dudley for reagents, Aaron Schetter and Ana Robles for statistical analysis, Barbara J. Taylor and Subhadra Banerjee for cell sorting, and Elisa Spillare for technical assistance. This research was supported in part by the Intramural Research Program of the NIH, NCI. B. Vojtesek was funded by grants from the Grant Agency of the Czech Republic (P301/11/1678 and P206/12/G151) and the RECAMO (CZ.1.05/2.1.00/03.0101). S.R. Pine was supported by the Biospecimen Repository Service (Julia Friedman), FACS Sorting (Arthur Roberts) Shared Resources of the CINJ (P30CA072720) and by a grant from the NIH, NCI (5K22CA140719). M.A. Blasco was funded by ERC Project TEL STEM CELL, FP7 Projects MARK-AGE and

EuroBATS, and other projects SAF2008-05384, CSD2007-00017 and S2010/BMD-2303 (Spain).

Received for publication April 8, 2013, and accepted in revised form September 10, 2013.

Address correspondence to: Curtis C. Harris, Laboratory of Human Carcinogenesis, Center for Cancer Research, National Cancer Institute, National Institutes of Health, 37 Convent Drive, Bethesda, Maryland 20892, USA. Phone: 301.496.2048; Fax: 301.496.0497; E-mail: Curtis_Harris@nih.gov.

1. Hayflick L. The limited in vitro lifetime of human diploid cell strains. *Exp Cell Res*. 1965;37:614–636.
2. Harley CB, Vaziri H, Counter CM, Allsopp RC. The telomere hypothesis of cellular aging. *Exp Gerontol*. 1992;27(4):375–382.
3. Bartkova J, et al. Oncogene-induced senescence is part of the tumorigenesis barrier imposed by DNA damage checkpoints. *Nature*. 2006;444(7119):633–637.
4. Newgard CB, Sharpless NE. Coming of age: molecular drivers of aging and therapeutic opportunities. *J Clin Invest*. 2013;123(3):946–950.
5. Montecino-Rodriguez E, Berent-Maoz B, Dorshkind K. Causes, consequences, and reversal of immune system aging. *J Clin Invest*. 2013; 123(3):958–965.
6. Tchkonia T, Zhu Y, van DJ, Campisi J, Kirkland JL. Cellular senescence and the senescent secretory phenotype: therapeutic opportunities. *J Clin Invest*. 2013;123(3):966–972.
7. Beltrami AP, Cesselli D, Beltrami CA. Stem cell senescence and regenerative paradigms. *Clin Pharmacol*. 2012;91(1):21–29.
8. Coppe JP, Desprez PY, Krtolica A, Campisi J. The senescence-associated secretory phenotype: the dark side of tumor suppression. *Annu Rev Pathol*. 2010;5:99–118.
9. Kuilman T, Peeper DS. Senescence-messaging secretome: SMS-ing cellular stress. *Nat Rev Cancer*. 2009; 9(2):81–94.
10. Kang TW, et al. Senescence surveillance of pre-malignant hepatocytes limits liver cancer development. *Nature*. 2011;479(7374):547–551.
11. Baker DJ, et al. Clearance of p16Ink4a-positive senescent cells delays ageing-associated disorders. *Nature*. 2011;479(7372):232–236.
12. Collado M, Blasco MA, Serrano M. Cellular senescence in cancer and aging. *Cell*. 2007;130(2):223–233.
13. Khoury MP, Bourdon JC. The isoforms of the p53 protein. *Cold Spring Harb Perspect Biol*. 2010; 2(3):a000927.
14. Bourdon JC, et al. p53 isoforms can regulate p53 transcriptional activity. *Genes Dev*. 2005; 19(18):2122–2137.
15. Fujita K, et al. p53 isoforms Δ133p53 and p53β are endogenous regulators of replicative cellular senescence. *Nat Cell Biol*. 2009;11(9):1135–1142.
16. Tang Y, et al. Downregulation of splicing factor SRSF3 induces p53β, an alternatively spliced isoform of p53 that promotes cellular senescence. *Oncogene*. 2013;32(22):2792–2798.
17. Parish ST, Wu JE, Effros RB. Sustained CD28 expression delays multiple features of replicative senescence in human CD8 T lymphocytes. *J Clin Immunol*. 2010;30(6):798–805.
18. Deeks SG. HIV infection, inflammation, immunosenescence, and aging. *Annu Rev Med*. 2011; 62:141–155.
19. Tarazona R, et al. Increased expression of NK cell markers on T lymphocytes in aging and chronic activation of the immune system reflects the accumulation of effector/senescent T cells. *Mech Ageing Dev*. 2000;121(1–3):77–88.
20. Effros RB, et al. Decline in CD28+ T cells in centenarians and in long-term T cell cultures: a possible cause for both in vivo and in vitro immunosenescence. *Exp Gerontol*. 1994;29(6):601–609.
21. Effros RB, Dagarag M, Spaulding C, Man J. The role of CD8+ T-cell replicative senescence in human aging. *Immunol Rev*. 2005;205:147–157.
22. Brenchley JM, et al. Expression of CD57 defines replicative senescence and antigen-induced apoptotic death of CD8+ T cells. *Blood*. 2003; 101(7):2711–2720.
23. Monteiro J, Batliwalla F, Ostrer H, Gregersen PK. Shortened telomeres in clonally expanded CD28-CD8+ T cells imply a replicative history that is distinct from their CD28+CD8+ counterparts. *J Immunol*. 1996;156(10):3587–3590.
24. McElhaney JE, Effros RB. Immunosenescence: what does it mean to health outcomes in older adults? *Curr Opin Immunol*. 2009;21(4):418–424.
25. Klebanoff CA, Gattinoni L, Restifo NP. CD8+ T-cell memory in tumor immunology and immunotherapy. *Immunol Rev*. 2006;211:214–224.
26. Effros RB, et al. Shortened telomeres in the expanded CD28-CD8+ cell subset in HIV disease implicate replicative senescence in HIV pathogenesis. *AIDS*. 1996;10(8):F17–F22.
27. Bodnar AG, et al. Extension of life-span by introduction of telomerase into normal human cells. *Science*. 1998;279(5349):349–352.
28. Collado M, et al. Tumour biology: senescence in premalignant tumours. *Nature*. 2005; 436(7051):642.
29. Narita M, et al. A novel role for high-mobility group a proteins in cellular senescence and heterochromatin formation. *Cell*. 2006;126(3):503–514.
30. Sedelnikova OA, Horikawa I, Zimonjic DB, Popescu NC, Bonner WM, Barrett JC. Senescing human cells and ageing mice accumulate DNA lesions with unrepairable double-strand breaks. *Nat Cell Biol*. 2004;6(2):168–170.
31. Marcel V, Khoury MP, Fernandes K, Diot A, Lane DP, Bourdon JC. Detecting p53 isoforms at protein level. *Methods Mol*. 2013;962:15–29.
32. Scheuring UJ, Sabzevari H, Theofilopoulos AN. Proliferative arrest and cell cycle regulation in CD8(+)CD28(-) versus CD8(+)CD28(+) T cells. *Hum Immunol*. 2002;63(11):1000–1009.
33. Rufer N, Dragowska W, Thornbury G, Roosnek E, Lansdorp PM. Telomere length dynamics in human lymphocyte subpopulations measured by flow cytometry. *Nat Biotechnol*. 1998;16(8):743–747.
34. Effros RB. Replicative senescence of CD8 T cells: effect on human ageing. *Exp Gerontol*. 2004; 39(4):517–524.
35. Chebel A, et al. Telomere uncapping during in vitro T-lymphocyte senescence. *Aging Cell*. 2009;8(1):52–64.
36. Boomer JS, Green JM. An enigmatic tail of CD28 signaling. *Cold Spring Harb Perspect Biol*. 2010; 2(8):a002436.
37. Bour-Jordan H, Esensten JH, Martinez-Llordella M, Penaranda C, Stumpf M, Bluestone JA. Intrinsic and extrinsic control of peripheral T-cell tolerance by costimulatory molecules of the CD28/ B7 family. *Immunol Rev*. 2011;241(1):180–205.
38. Ward SG. CD28: a signalling perspective. *Biochem J*. 1996;318(pt 2):361–377.
39. Djavaheri-Mergny M, et al. NF-κB activation represses tumor necrosis factor-alpha-induced autophagy. *J Biol Chem*. 2006;281(41):30373–30382.
40. Nazio F, et al. mTOR inhibits autophagy by controlling ULK1 ubiquitylation, self-association and function through AMBRA1 and TRAF6. *Nat Cell Biol*. 2013;15(4):406–416.
41. Montes CL, et al. Tumor-induced senescent T cells with suppressor function: a potential form of tumor immune evasion. *Cancer Res*. 2008; 68(3):870–879.
42. Yang OO, Lin H, Dagarag M, Ng HL, Effros RB, Uittenbogaart CH. Decreased perforin and granzyme B expression in senescent HIV-1-specific cytotoxic T lymphocytes. *Virology*. 2005;332(1):16–19.
43. Filaci G, et al. Nonantigen specific CD8+ T suppressor lymphocytes originate from CD8+CD28- T cells and inhibit both T-cell proliferation and CTL function. *Hum Immunol*. 2004;65(2):142–156.
44. Effros RB. Replicative senescence: the final stage of memory T cell differentiation? *Curr HIV Res*. 2003; 1(2):153–165.
45. Bestilny LJ, Gill MJ, Mody CH, Riabowol KT. Accelerated replicative senescence of the peripheral immune system induced by HIV infection. *AIDS*. 2000;14(7):771–780.
46. Chen DS, Irving BA, Hodi FS. Molecular pathways: next-generation immunotherapy — inhibiting programmed death-ligand 1 and programmed death-1. *Clin Cancer Res*. 2012;18(24):6580–6587.
47. Topalian SL, et al. Safety, activity, and immune correlates of anti-PD-1 antibody in cancer. *N Engl J Med*. 2012;366(26):2443–2454.
48. Lapasset L, et al. Rejuvenating senescent and centenarian human cells by reprogramming through the pluripotent state. *Genes Dev*. 2011; 25(21):2248–2253.
49. Vizcardo R, et al. Regeneration of human tumor antigen-specific T cells from iPSCs derived from mature CD8(+) T cells. *Cell Stem Cell*. 2013; 12(1):31–36.
50. Gattinoni L, Klebanoff CA, Restifo NP. Paths to stemness: building the ultimate antitumour T cell. *Nat Rev Cancer*. 2012;12(10):671–684.
51. Eminli S, et al. Differentiation stage determines potential of hematopoietic cells for reprogramming into induced pluripotent stem cells. *Nat Genet*. 2009;41(9):968–976.
52. SM Studer L. Cell fate plug and play: direct reprogramming and induced pluripotency. *Cell*. 2011; 145(6):827–830.
53. Nishimura T, et al. Generation of rejuvenated antigen-specific T cells by reprogramming to pluripotency and redifferentiation. *Cell Stem Cell*. 2013; 12(1):114–126.
54. Pine SR, Ryan BM, Varticovski L, Robles AI, Harris CC. Microenvironmental modulation of asymmetric cell division in human lung cancer cells. *Proc Natl Acad Sci U S A*. 2010;107(5):2195–2200.
55. Perillo NL, Walford RL, Newman MA, Effros RB. Human T lymphocytes possess a limited in vitro life span. *Exp Gerontol*. 1989;24(3):177–187.
56. Yang S, Dudley ME, Rosenberg SA, Morgan RA. A simplified method for the clinical-scale generation of central memory-like CD8+ T cells after transduction with lentiviral vectors encoding antitumor antigen T-cell receptors. *J Immunother*. 2010; 33(6):648–658.
57. Brzezinska A, Magalska A, Sikora E. Proliferation of CD8+ in culture of human T cells derived from peripheral blood of adult donors and cord blood of newborns. *Mech Ageing Dev*. 2003;124(4):379–387.
58. Canela A, Vera E, Klatt P, Blasco MA. High-throughput telomere length quantification by FISH and its application to human population studies. *Proc Natl Acad Sci U S A*. 2007;104(13):5300–5305.
59. Cohen S, Kamarck T, Mermelstein R. A global measure of perceived stress. *J Health Soc Behav*. 1983; 24(4):385–396.